JOURNAL OF ENVIRONMENTAL SCIENCES 138 (2024) 112–120

Available online at www.sciencedirect.com

ScienceDirect

www.elsevier.com/locate/jes

JES JOURNAL OF ENVIRONMENTAL SCIENCES

www.jesc.ac.cn

Photo-thermal synergistic excitation: Feasible strategy to detect ethanol for wide bandgap ZIF-8 at low work temperature

Shuhao Shi[1], *Qian Du*[1], *Ming Hou*[1], *Xiaolei Ye*[3,*], *Li Yang*[1,2,*], *Shenghui Guo*[1], *Jianhong Yi*[4], *Ullah Ehsan*[1], *Hongbo Zeng*[2]

[1] *State Key Laboratory of Complex Nonferrous Metal Resources Clean Utilization, Faculty of Metallurgical and Energy Engineering, Kunming University of Science and Technology, Kunming 650093, China*
[2] *Department of Chemical and Materials Engineering, University of Alberta, Edmonton T6G 2V4, Canada*
[3] *FEMTO -ST Institute (UMR CNRS 6174), Université de Bourgogne Franche-Comté (UBFC), Université de technologie de Belfort Montbéliard (UTBM), Site de Montbéliard, Belfort F-90010, France*
[4] *Faculty of Materials Science and Engineering, Kunming University of Science and Technology, Kunming 650093, China*

ARTICLE INFO

Article history:
Received 26 September 2022
Revised 28 February 2023
Accepted 28 February 2023
Available online 10 March 2023

Keywords:
ZIF-8 material
Photo-thermal synergistic excitation
UV-light irradiation
Photon-generated electron and hole
Gas-sensitive property

ABSTRACT

Zeolitic Imidazolate Framework-8 (ZIF-8) material was prepared by chemical precipitation method. The microstructure and physical properties of the as-prepared samples were characterized by XRD, BET, FESEM and UV spectrophotometer. The self-made four-channel measurement device was used to test the gas sensitivity of ZIF-8 material toward ethanol gas under photo-thermal synergistic excitation. The results showed that the sample was typical ZIF-8 (E_g = 4.96 eV) with a regular dodecahedron shape and the specific surface is up to 1793 m^2/g. The as-prepared ZIF-8 has a gas response value of 55.04 to 100 ppm ethanol at 75°C and it shows good gas sensing selectivity and repeated stability. The excellent gas sensitivity can be attributed to the increase of free electron concentration in the ZIF-8 conduction band by photo-thermal synergistic excitation, and the large specific surface area of ZIF-8 material provides more active sites for gas-solid surface reaction. The reaction mechanism of ZIF-8 material under multi-field excitation was also discussed.

Introduction

In recent decades, with the development of industry and technology, humans have been inevitably exposed to Volatile Organic Compounds (VOCs) gases (Hallquist et al., 2009; Harrison and Yin, 2000; Hou et al., 2021; Mirzaei et al., 2016; Tomoda et al., 2004), and ethanol gas is one of the typical VOCs. Prolonged heavy consumption of ethanol gas can cause significant permanent damage to the liver and other organs (Young et al., 2012). Ethanol vapor easily burns or explodes under high temperatures or fire, which is seriously harmful to the environment and human health. Thus, it is important and urgent to develop a high-performance and portable gas sensor to detect and monitor the leakage of VOCs like ethanol.

Metal Organic Frameworks (MOFs) have the advantages of high porosity, stability, and high adsorption surface area (Lu et al., 2012; Tan et al., 2021). These characteristics make MOFs materials can be used in many fields, including: gas sen-

* Corresponding authors.
E-mails: xiaolei.ye@utbm.fr (X. Ye), yanglikmust@163.com (L. Yang).

https://doi.org/10.1016/j.jes.2023.02.056
1001-0742/

sor (Fang et al., 2018), catalysis (Dang et al., 2020; Nguyen et al., 2019), fuel storage (Ahmed et al., 2019), electrochemical sensor (Li et al., 2022), drug delivery (Dang et al., 2020), gas storage and separation (Li et al., 2018). Since Park et al. (2006) reported a series of synthesis methods and structures of ZIFs materials in 2006, the ZIFs series has been developed rapidly. Amongst them, ZIF-8 is a material with good high temperature and chemical stability, which advantages are small pores and large pores arranged in a sodalite (SOD) zeolite-type structure (Lu et al., 2012). The large specific surface area made it attract a lot of attention in the field of gas-sensitive materials. Xing et al. developed bimetallic ZIF-8 (Zn@Co)-based 1DPCs vapor sensors. They studied the recovery time and response time of the sample at 600 ppm MCB vapor and 200°C, which were about 9.5 s and 600 ms. After 30 days of storage, it exhibits great reversibility and stability (Xing et al., 2021). Xiong et al. (2017) prepared porous ZnO-decorated Co_3O_4 hollow polyhedron with a band gap of 3.37 eV by thermal decomposition deposition method of ZIF-67 templates. The response of the porous ZnO–Co_3O_4 hollow polyhedrons to 1000 ppm ethanol was 106, more than 19.7 times of pure Co_3O_4 at 200°C. Ostad et al. (2021) found that ZnO/ZIF-8 photocatalyst's features the oxygen vacancies in ZnO NPs, the permanent generation of electron-hole pairs, and an efficient charge-carrier separation due to formation of type II heterojunctions demonstrated higher. Although ZnO/ZIF-8 composite has very narrow band gap energy compared to pristine ZIF-8, but ZnO/ZIF-8 composite is still in the wide band gap semiconductor range with a band gap of 3.23 eV. The work of Wu et al. also proves this point, the ZnO@ZIF-8 core-shell nanorods film had a richer oxygen vacancy than that of the raw ZnO nanorods film. They investigated the gas sensor properties of ZnO@ZIF-8 nanorods film prepped prepared by the chemical solution deposition method. Nanowires maintained a relative H_2 sensitivity ($R_a/R_g = 2.79$, for 50 ppm) at 200°C, and selectivity of H_2 over CO was observed The CO gas molecules were unable to pass through the small pores of ZIF-8, which significantly decreased the CO response of the ZnO@ZIF-8 nanorods film. When the temperature decreased from 250 to 200°C, the ZnO@ZIF-8 nanorods sensor showed no response for CO, which indicated the stronger suppression effect on the CO sensitivity (Wu et al., 2017). Based on the above studies, it is confirmed that ZIF-8 material has good gas sensing response to the target gas at high concentration and high working temperature. Due to the wide-bandgap semiconductor property of ZIF-8, it is often required to work at a high temperature (more than 200°C). However, most of the industrial applications demand the gas sensors to be operated at low temperature (Shukla et al., 2005). The high temperature can cause high power consumption and will limit the application of gas sensitive materials in portable devices (Hou et al., 2021). Thus, it is important to explore and develop sensors that can operate at low temperatures.

Based on the working principle of the resistive semiconductor gas sensor, it was found that the irradiation of the sensing material was also one of the choices of the free carrier excitation. The light energy irradiation makes the valence band (VB) electron transition to obtain free electrons (Cui et al., 2016; Karaduman et al., 2014; Yu et al., 2022). Based on the above statements, photoexcitation is a feasible and effective method to improve carrier concentration and decrease the working temperature (Tielrooij et al., 2013). Chen et al. developed an Au−MoS_2 gas sensor that can respond to NO_2 with gas concentration of 10 ppb under 530 nm illumination (Chen et al., 2021). They found that visible light increased the surface carrier concentration of MoS_2, which led to an improvement in the performance of the gas sensor. Yang et al. founded that TiO_2 has a good gas sensing response to CO gas under the assistance of ultraviolet light irradiation (Yang et al., 2003). They found that the intensity of UV light has positive effect on the gas sensing properties. Tomić et al. developed an APTES@WO_3-x sensor that can responses to nitrogen dioxide and ethanol increased approximately 17 and 20 times under UV-irradiation at room temperature (25°C) . That APTES@WO_3-x with a band gap of 3.37 eV (Tomić et al., 2021). They found that the chemical interaction between ethanol and nitrogen dioxide, and the transfer of electrons to WO_3-x were carried out under UV-light excitation. This indicates that photoexcitation is beneficial to the transport of carriers in wide-bandgap semiconductor materials, thereby improving the gas sensitivity of gas-sensing materials. Hence, photo-thermal synergistic excitation will be expected to be an effective process to decrease the working temperature of ZIF-8 and improve the gas sensitivity. As far as I know, this is the first report on the gas sensing performance of pure ZIF-8 under photo-thermal synergistic excitation.

In this work, ZIF-8 material was prepared by chemical precipitation method, and the gas sensitivity of the as-prepared ZIF-8 under photo-thermal synergistic excitation were investigated. The free electron concentration in the ZIF-8 conduction band can be increased by photo-thermal synergistic excitation. The large specific surface area of ZIF-8 material provides more active sites for gas-solid surface reactions. The reaction mechanism of ZIF-8 material under multi-field excitation was also discussed, which was expected to provide a theoretical basis for ZIF-8 material in the field of cryogenic sensors.

1. Experimental

1.1. *Methods of sample preparation*

As far as we known, there are several reports about the preparation of ZIF-8 materials. According to the experimental conditions, we chose chemical precipitation method (Lu and Hupp, 2010). $Zn(NO_3)_2{\cdot}6H_2O$ (1485 mg, 4.99 mmol) was added into 20 mL of methanol solution at room temperature and sonicated for 3 min until it was completely dissolved. 2-Methylimidazole (1642 mg, 20.00 mmol) was added to another beaker containing 20 mL of methanol and ultrasonic 3 min to make it fully dissolved. The obtained two colorless solutions were thoroughly mixed, and the ultrasonic treatment was continued for 2 min, so that the two solutions were completely mixed uniformly. The homogeneously mixed solution was then stand in a dry room temperature environment for 24 h. A white precipitate was then obtained. Then, the obtained white precipitate was washed with ethanol by centrifu-

gation, placed in vacuum drying oven, and dried overnight at a constant temperature of 70°C to finally obtain ZIF-8 material.

1.2. Samples characterization

X-ray (X'Pert3 MRD, Netherlands) diffraction to determine the crystalline phase of the as-prepared samples with the 2θ range from 5° to 40° and speed of 5°/min. The microscopic morphologies of the as-prepared samples were observed using field emission scanning electron microscope (FESEM, Nova NanoSEM 450, America). The pore structure characteristics of the as-prepared samples were obtained by N_2 isothermal adsorption desorption test, and the highly-specific surface area of the samples was calculated by BET theoretical model. The luminescence spectra of the as-prepared samples were investigated by an ultraviolet spectrophotometer (SHIMADZU UV-2600/2700, Japan) and the band gap value was calculated by plotting and calculated.

1.3. Performance test of gas-sensor

The sample preparation for gas sensing performance test was prepared as follows: First, the platinum electrode paste was printed on the Al_2O_3 basement (6 × 30 mm) by silk-screen printing to prepare a measuring resistance sensor, and then the Al_2O_3 substrate was dried in an oven. Then, the sample was printed on the electrode chip by silk-screen printing to form a sensing film with a thickness of approximately 5–10 μm, and then put the electrode into the tube furnace, heated in air to 350°C for 2 h to obtain samples for subsequent testing.

Gas sensing performance test was performed on a self-made four-channel measurement device (SD101, Kunming University of Science and Technology). First, the UV LED module was inserted, and then the fabricated chip was placed in a closed cavity. After switching on the device and PC side gas sensing test software, the "Add light" was selected in the four-channel gas sensing performance test software. After the UV LED module in the cavity is stable, the chip was then different gases and gas sensing tests at different concentrations were performed.

The gas response value is calculated by the following formula:

$$S = \frac{R_g - R_a}{R_a} \times 100\% \quad (1)$$

where, S (%) is sensitivity which is used to evaluate the sensitivity of gas sensitive materials to target gases, R_g is the stable resistance value of the gas sensitive material after adsorbing the target gas, R_a is the resistance value of the gas sensitive material when it is stable in dry air.

2. Results and discussion

As shown in Fig. 1, the synthesized samples have a regular dodecahedron shape. The morphology of the nanoparticles was observed by FESEM. The surface of the as-synthesized sample is flat and smooth, with an average length about 300 nm, which is in line with the morphology of ZIF-8 material, and the results are displayed in Fig. 1b. The synthesized ZIF-8 material sample was tested by XRD analysis, and the results are displayed in Appendix A Fig. S1. The samples have obvious diffraction peaks at 7.3°, 10.3°, 12.7° and 18.0°, which correspond to the (110), (200), (211) and (222) crystal planes of ZIF-8 material (Li and Zeng, 2013) respectively. ZIF-8 material was successfully prepared by the chemical precipitation method at room temperature and normal pressure (1.013×10^5 Pa), which is proved by FESEM and XRD analysis.

One of the properties affecting gas sensitive materials is specific surface area. In general, larger the specific surface area, better the gas sensitivity. Information on the pore structure of the ZIF-8 material was explored using the N_2 isotherm adsorption and desorption curves, as shown in Appendix A Fig. S2. The ZIF-8 material specific surface area was calculated as high as 1793 m^2/g by the BET theoretical model.

Because of microporous structure, ZIF-8 can interact strongly with N_2. The Y axis of the low-pressure end indicates that the material has a strong force with nitrogen. When there are more micropores, the adsorption curve starts to be I-shaped due to the strong adsorption potential in the micropores. Low pressure ends off X axis shows weak force with material.

The band gap width of ZIF-8 semiconductor material, its light absorption ability in the wavelength range of 200–800 nm was explored with an ultraviolet spectrophotometer. Fig. 2a shows that ZIF-8 material has a strong absorption capacity for light with a wavelength of 219 nm. Light with a wavelength of 219 nm is in the UV wavelength range. Based on the test, the light sources used in the subsequent gas sensing test under the condition of combined excitation of light and heat are all ultraviolet light sources. Fig. 2b also illustrates the calculated band gap energy (E_g) from the tangent over the curve of $(Ah\nu)^{0.5}$ versus photo-energy $h\nu$ based on Tauc plot (Chandra and Nath, 2017; Chen et al., 2019; Goyal et al., 2018). In this plot, h is defined as Planck's constant, A is the absorption coefficient obtained from Kubelka-Munk transformation function (Ahsan et al., 2017), and ν is assigned to frequency. The calculated bandgap of ZIF-8 material is $E_g = 4.96$ eV, proving that ZIF-8 material is a wide-bandgap semiconductor material. It is proved that the gas sensing response can be improved by increasing the external field effect of photoexcitation to provide more photogenerated electron-hole pairs for the gas-solid reaction on the surface of ZIF-8 material.

As shown in Fig. 3, the gas sensing performance of the ZIF-8 material was tested to 100 ppm different types of gases (only NO_2 is 10 ppm) at 300°C. The ZIF-8 material can response to various target gases at high temperatures (300°C) and has relatively good selectivity to small molecules of CO_2. The aperture size of ZIF-8 material is about 0.34 nm, it can produce effective gas permeability to small molecules of CO_2 (0.33 nm) with a similar aperture size (Liu et al., 2011). However, compared with traditional metal-oxide-semiconductor gas sensing materials, ZIF-8 material does not show particularly excellent gas-sensing responses. Even though ZIF-8 material possesses many unsaturated coordination metal active sites and a high specific surface area, its weak electrical conductivity significantly reduces its gas sensing capability.

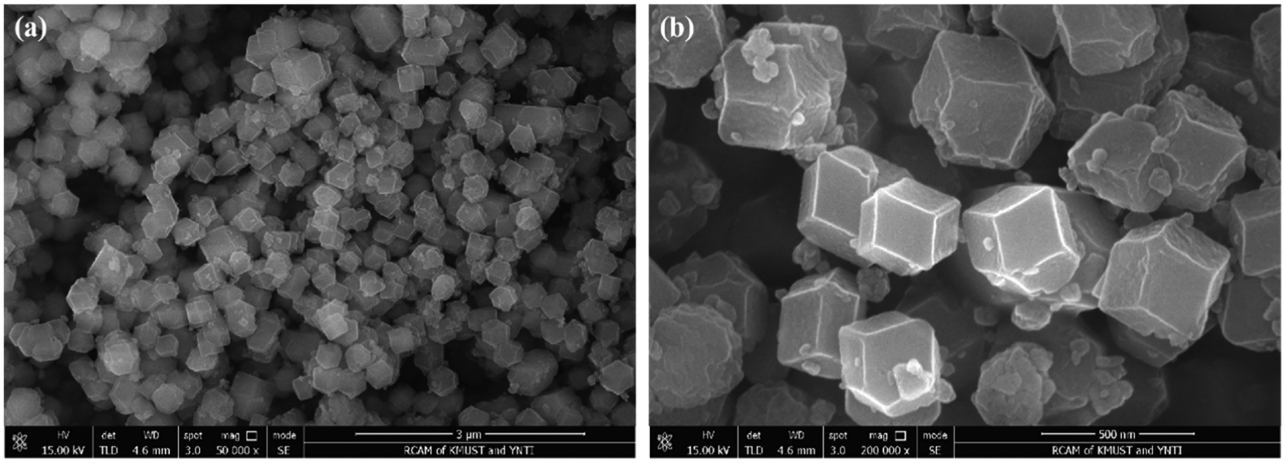

Fig. 1 – FESEM morphology (a) and structure (b) of ZIF-8 material.

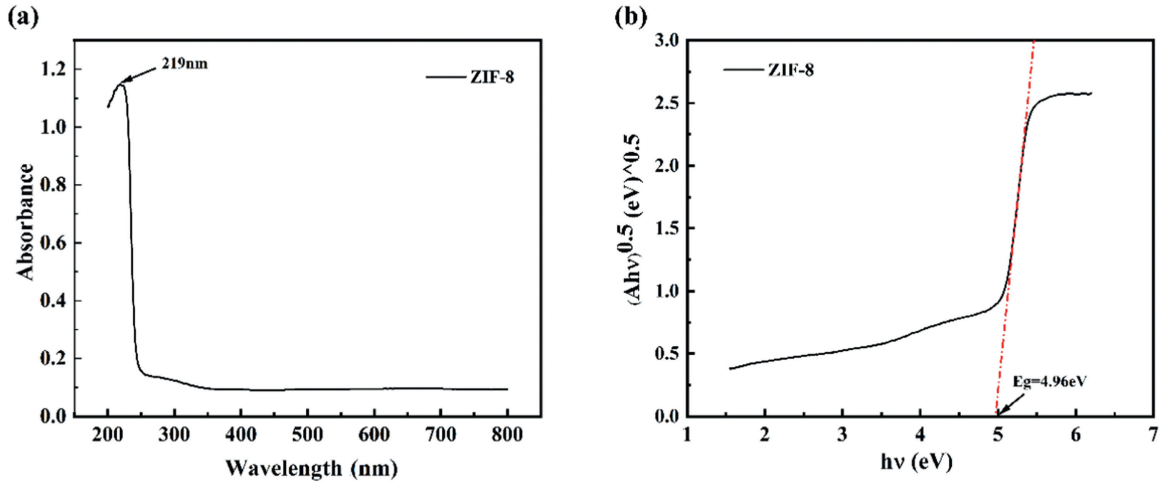

Fig. 2 – (a) UV spectrophotometric test spectrum of ZIF-8 material, (b) band gap of ZIF-8 material.

In accordance with the observations, UV-light excitation with higher energy can reduce the response-recovery time of gas sensing materials. As a result, multiple gas sensing cycle tests on ZIF-8 material were performed at 300°C under the conditions of single thermal excitation and combined photothermal excitation. The gas sensing response and the recovery curve of ZIF-8 material under two excitation conditions were obtained, as shown in Fig. 4. UV-light excitation with higher energy can indeed reduce the response time and recovery time of the ZIF-8 material (Fig. 4a and Fig. 4b). Under the condition of photo-thermal synergistic excitation, the ZIF-8 material exhibits a response time of 59 sec and a recovery time of 125 sec to 100 ppm ethanol gas at 300°C, both of which are much shorter than the response-recovery time under thermal excitation alone.

Studying the optimal working temperature is the key for the gas sensing material to exhibit its excellent gas sensing performance. The gas sensing response of ZIF-8 material to 100 ppm ethanol at 25~350°C was tested under the condition of photo-thermal synergistic excitation, as shown in Fig. 5. The ZIF-8 material exhibits a specific gas sensing response to 100 ppm ethanol at room temperature when subjected to optical excitation; the response value is 24.43. It is worth noting that the response of ZIF-8 material to 100 ppm ethanol is only 18.98 at a 300°C operating temperature. However, the ZIF-8 material had almost no response to 100 ppm ethanol at room temperature. This study shows that the conditions of optical excitation can indeed reduce the working temperature of gas sensing materials so that they can produce ideal gas sensing responses at a lower temperature.

As shown in Fig. 5, under the condition of photo-thermal synergistic excitation, the ZIF-8 material is still greatly affected by temperature, and the gas sensing sensitivity of the ZIF-8 material to 100 ppm ethanol increases with the increase of temperature. Photo-thermal synergistic excitation can provide more electron-hole pairs at lower temperatures, improve the electrical conductivity of ZIF-8 material and improve the ability of ZIF-8 material to conduct gas-solid reaction with ethanol gas. Therefore, the gas sensing response of ZIF-8 material to 100 ppm ethanol increased relatively rapidly in the range of 25–75°C. With the increase of temperature, optical excitation can still provide a significant number of photogen-

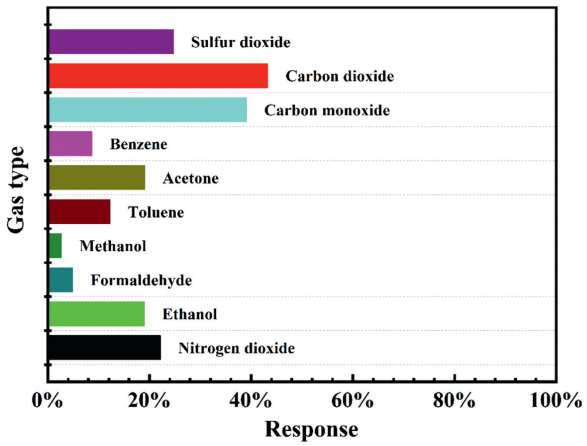

Fig. 3 – Gas responses of ZIF-8 material toward 100 ppm of different target gases at 300°C, under thermal excitation (only NO_2 was 10 ppm).

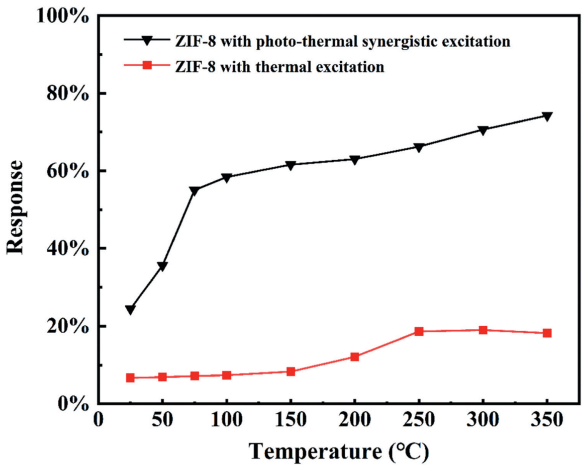

Fig. 5 – Gas responses of ZIF-8 material toward 100 ppm ethanol gas at different operating temperatures.

erated electron hole pairs for gas-solid reaction. Due to the wide-bandgap semiconductor property of ZIF-8, it is often required to work at high temperature (more than 200°C). On the one hand, an increase in temperature increases the recombination of photogenerated electron hole pairs. On the other hand, higher working temperatures will accelerate the recombination of photogenerated electron hole pairs and also affect the adsorption of ethanol gas on ZIF-8 material, resulting in the desorption of ethanol gas adsorbed on the material's surface, which impedes the smooth progress of gas-solid reaction. Under the action of accelerating the recombination of photogenerated electron hole pairs and desorption of ethanol gas adsorbed on the surface of the material, the gas sensing response finally showed a slow growth trend.

The "speed-up turning point" of 75°C shown in Fig. 5 was selected as the optimal working temperature of ZIF-8 material for 100 ppm ethanol gas because thermal excitation at this temperature can still enhance the chemical activity of the ZIF-8 material and make its surface adsorb more oxygen anions. In comparison previous work, ZIF-8 material has excellent gas sensing response to 100 ppm ethanol gas under photo-thermal synergistic excitation condition. The comparison results are shown in Table 1.

Excellent selectivity is another important characteristic for evaluating the gas sensing properties of materials. Herein, the of ZIF-8 material to 100 ppm different target of gases at 75°C were selected. Amongst them, they include macromolecular VOCs, ethanol, toluene, methanol, formaldehyde and benzene, as well as small molecules of CO_2 and SO_2. The ultimate goal is to determine whether the ZIF-8 material has good selectivity. As shown in Fig. 6, the ZIF-8 material has good selectivity for 100 ppm ethanol gas because of the large pore size of the 1.16 nm in the ZIF-8 material, which can adsorb macromolecular organics (Yan et al., 2014). It can be seen that the large pore size of the ZIF-8 material plays a major role in the adsorption and desorption of the target gas under the combined excitation of light and heat.

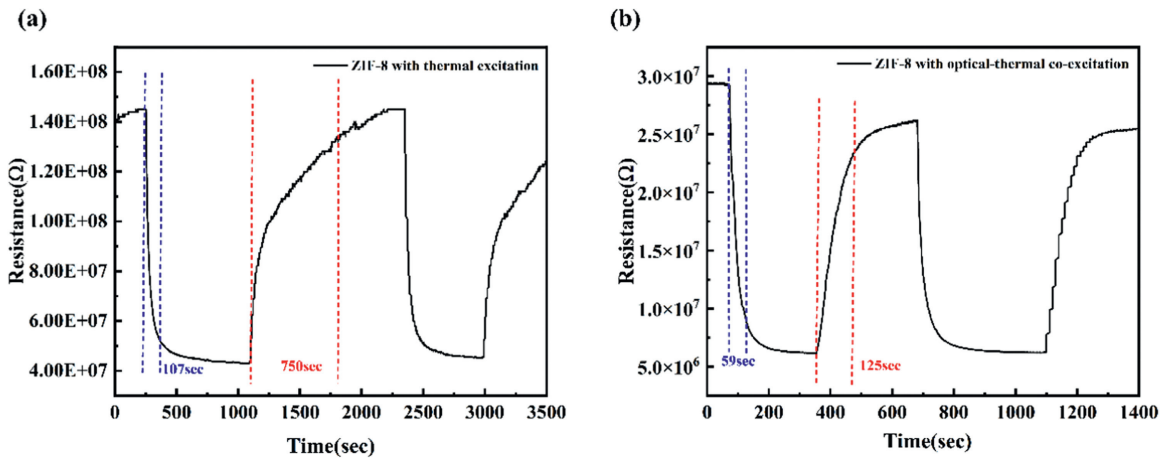

Fig. 4 – Response-recovery curves of ZIF-8 material toward 100 ppm ethanol gas at 300 °C. (a) thermal excitation, (b) under the condition of photo-thermal synergistic excitation.

Table 1 – Gas responses of ZIF-8 material to ethanol gas compared with other works under the condition of photo-thermal synergistic excitation.

Sensing material	Operating temperature	Sensitivity	Field condition	Refs.
ZnO nanotubes	90°C	34@100 ppm	thermal excitation	(Hsueh et al., 2008)
α-Fe_2O_3 nanoparticles	150°C	14.5@100 ppm	thermal excitation	(Shoorangiz et al., 2021)
5 at% CeO_2/CdS composite exhibited	161°C	52@100 ppm	thermal excitation	(Li et al., 2017)
SnS/SnS_2 nanoparticles	200°C	30.12@100 ppm	thermal excitation	(Zhang et al., 2020)
Vertically Aligned ZnO Nanorod	300°C	3.11@100 ppm	thermal excitation	(Ahn et al., 2010)
ZnO nanowires	300°C	26@100 ppm	thermal excitation	(Hsueh et al., 2007)
ZIF-8 material	75°C	55.04@100 ppm	photo-thermal synergistic excitation	This work

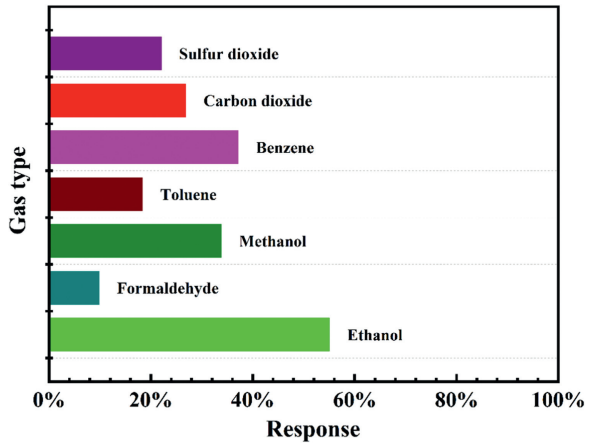

Fig. 6 – The gas responses of ZIF-8 material to 100 ppm different target gases at 75°C, under the condition of photo-thermal synergistic excitation.

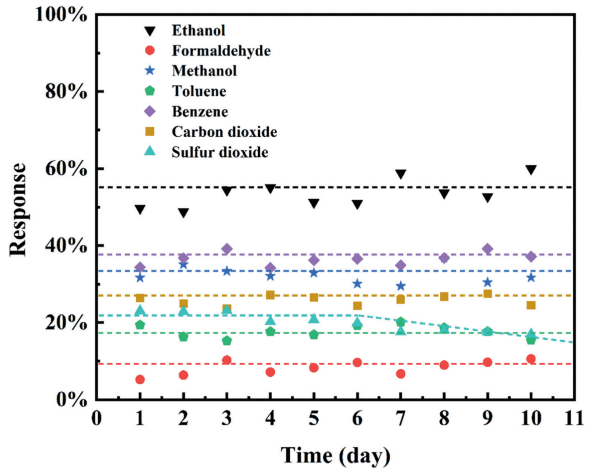

Fig. 7 – Long-term stability experiment of ZIF-8 material to 100 ppm different target gases at 75°C, under the condition of photo-thermal synergistic excitation.

The long-term stability of gas-sensitive materials is an important guarantee for their wide application. As shows in Fig. 7, the long-term stability tests on the ZIF-8 material were also performed. During this period, the gas sensing test of ZIF-8 material under the combined excitation of light and heat was carried out once a day for ten consecutive days. The gas sensing response value of ZIF-8 material to 100 ppm ethanol gas fluctuates around 55.04, and the fluctuation difference is no more than 10%, which proves that ZIF-8 material is a stable low-temperature ethanol gas sensor.

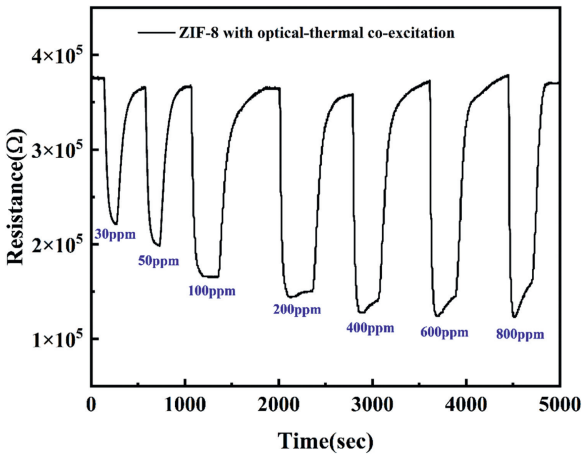

Fig. 8 – Dynamic response-recovery curve of ZIF-8 material to different concentrations ethanol gas at 75°C under the condition of photo-thermal synergistic excitation.

The relationship between the gas sensing response of the gas sensing material and the target gas concentration at the optimum operating temperature is also an important criterion for measuring its gas sensing performance. The gas sensitivity of ZIF-8 material to different concentrations of ethanol gas was tested, and the dynamic response-recovery curve of ethanol gas concentration and ZIF-8 gas sensing material was obtained under the condition of photo-thermal synergistic excitation at the operating temperature of 75°C with concentrations of 30, 50, 100, 200, 400, 600, and 800 ppm. The results are displayed in Fig. 8. ZIF-8 material exhibits a positive correlation with the concentration of ethanol gas in the range of 30–800 ppm at working temperature of 75°C, and its gas sensing response increases as the concentration of ethanol gas increases. Under the condition of photo-thermal synergistic excitation, the ZIF-8 material has a sensitivity value of 55.04 to 100 ppm ethanol gas at working temperature of 75°C, which is more than other ZIF-8 based materials under separate thermal excitation and optimal

working temperature. For example, Ren et al. have prepared ZnO@ZIF-8 core-shell microsphere gas sensing material with a gas sensing response value of 35.90 to 100 ppm ethanol gas at the optimum working temperature of 160°C (Ren et al., 2019). However, the gas sensing response of ZIF-8 material in this study to the same concentration of ethanol gas under the condition of photo-thermal synergistic excitation and the working temperature of 75°C is more than 1.6 times than that of the work by Ren et al. (2019) . In addition, it can be seen from the gas sensing test cycle of each concentration that the ZIF-8 material has a repeatable steady-state response and recovery ability to ethanol gas, and the ZIF-8 material is a wide-bandgap n-type semiconductor material. At the same time, the ZIF-8 material has a lower detection limit for ethanol gas under the conditions of photo-thermal synergistic excitation and heat and a working temperature of 75°C.

In summary, the working temperature of 75°C was selected as the optimal working temperature of ZIF-8 material for 100 ppm ethanol, and under the condition of photo-thermal synergistic excitation of improving the gas sensitivity of ZIF-8 material to ethanol gas response, enabling it to have excellent gas sensing performance under lower temperature conditions, as shown in Appendix A Fig. S3.

The gas sensing reaction of gas sensing materials to target gases is a multi-step and complex process. The effect of photothermal synergistic excitation on gas sensing materials and the corresponding gas sensing reaction mechanism are explained by the electron depletion layer theory. Firstly, the electrons in its valence band will be excited to the conduction band to become free electrons under the condition of thermal excitation alone, when the ZIF-8 material is in dry air. At this point, due to the large electronegativity of ZIF-8 material surface, oxygen molecules will capture free electrons from its surface and adsorb on it, resulting in chemical adsorption of oxygen, as shown in Appendix A Fig. S3b. The types of adsorbed oxygen at low temperatures are usually in the form of O_2^- (Barsan and Weimar, 2001) from the following formula:

$$O_2 + e^- \leftrightarrow O_2^- \quad (2)$$

At this time, a large number of oxygen negative ions are adsorbed on the surface of ZIF-8 material, and the internal electrons of the material are reduced. A depletion layer is induced on the surface to form an internal electric field, resulting in a relatively large resistance of the material itself. After the addition of UV-light excitation, more electrons in the valence band of ZIF-8 materials were excited to transition to the conduction band, and holes were left in the valence band, and the resistance value was further increased, as shown in Appendix A Fig. S3c. Ultimately, the resistance of ZIF-8 material will also reach a stable state after the above charge migration reaches equilibrium under the condition of photo-thermal synergistic excitation.

When ZIF-8 material is exposed to an ethanol gas molecular environment, ethanol molecules react with oxygen negative ions on the surface of the ZIF-8 material as follows:

$$CH_3CH_2OH + 3O_2^- \rightarrow 2CO_2 + 3H_2O + 3e^- \quad (3)$$

This gas sensing reaction will produce and release a large number of electrons, some of which will be injected into the conduction band again, narrowing the depletion layer and thus reducing the resistance of ZIF-8 material. However, some of the electrons will be combined with the holes generated by UV-light excitation to narrow the depletion layer again and promote the above gas sensing reactions, further reducing the resistance of ZIF-8 materials. These two processes make the resistance difference of ZIF-8 material larger before and after exposure to ethanol gas, so that ZIF-8 material can have a higher gas sensing response to 100 ppm ethanol at a lower temperature.

In summary, after the condition of photo-thermal synergistic excitation, the photogenerated electron-hole pairs generated by ZIF-8 material will play a positive effect on the improvement of its gas sensing performance.

3. Conclusions

ZIF-8 material was prepared by the room temperature and normal pressure synthesis method and has about 1793 m^2/g high specific surface area. The ZIF-8 material could absorb the ultraviolet light source with a wavelength of 219 nm, and its band-gap is 4.96 eV. Under the condition of photothermal synergistic excitation, ZIF-8 has excellent gas sensing response to 100 ppm ethanol at 75°C, and the response value is 55.04. For formaldehyde (about 9.8), methanol (about 33.8), toluene (about 18.32), benzene (about 37.13), carbon dioxide (about 26.82) and sulfur dioxide (about 22.02), the gas sensitivity values were less than 40 and showed good gas sensing selectivity. At the same time, gas sensing tests were conducted once a day for ten consecutive days. The fluctuation difference was no more than 10%. UV-light excitation causes a large number of photogenerated electron-hole pairs in ZIF-8 material, which promotes the reaction of ethanol gas molecules with oxygen anion on the surface of ZIF-8 material and improves the gas sensing properties. ZIF-8 material can have excellent ethanol gas sensing response in a low temperature working environment under the condition of photo-thermal synergistic excitation.

Declaration of Competing Interest

All authors agree with this submission and declare that there are no competing of financial interest in our submission.

Acknowledgements

This work was supported by the National Natural Science Foundation of China (No. 51864028); the Yunnan Province Science and Technology Major Project for Materials Genetic Engineering of Rare and Precious Metal (No. 202002AB080001); the Yunnan Province Funds for Distinguished Young Scientists, (No. 2019FJ005); the Science Research Foundation of Yunnan Provincial Education Department (No. 2022J0441); the Sichuan Science and Technology Program (No. 22QYCX0097).

Appendix A Supplementary data

Supplementary material associated with this article can be found, in the online version, at doi:10.1016/j.jes.2023.02.056.

References

Ahmed, A., Seth, S., Purewal, J., Wong-Foy, A.G., Veenstra, M., Matzger, A.J., et al., 2019. Exceptional hydrogen storage achieved by screening nearly half a million metal-organic frameworks. Nat. Commun. 10 (1), 1568.

Ahn, H., Park, J.H., Kim, S.B., Jee, S.H., Yoon, Y.S., Kim, D.J., 2010. Vertically aligned ZnO nanorod sensor on flexible substrate for ethanol gas monitoring. Electrochem. Solid-State Lett. 13 (11), J125.

Ahsan, R., Khan, M.Z.R., Basith, M.A., 2017. Determination of optical band gap of powder-form nanomaterials with improved accuracy. J. Nanophotonics 11 (4), 046016.

Barsan, N., Weimar, U., 2001. Conduction model of metal oxide gas sensors. J. Electroceram. 7, 143–167.

Chandra, R., Nath, M., 2017. Multi-core–shell TiO_2NPs@ ZIF-8 composite for enhanced photocatalytic degradation and adsorption of methylene blue and Rhodamine-B. ChemistrySelect 2 (25), 7711–7722.

Chen, W.Q., Li, L.Y., Li, L., Qiu, W.H., Tang, L., Xu, L., et al., 2019. MoS_2/ZIF-8 hybrid materials for environmental catalysis: solar-driven antibiotic-degradation engineering. Engineering 5 (4), 755–767.

Chen, P., Hu, J., Yin, M., Bai, W., Chen, X., Zhang, Y., 2021. MoS_2 nanoflowers decorated with au nanoparticles for visible-light-enhanced gas sensing. ACS Appl. Nano Mater. 4 (6), 5981–5991.

Cui, J., Shi, L., Xie, T., Wang, D., Lin, Y., 2016. UV-light illumination room temperature HCHO gas-sensing mechanism of ZnO with different nanostructures. Sens. Actuators B 227, 220–226.

Dang, M.H.D., Nguyen, T.T.M., Nguyen, L.H.T., Nguyen, T.T.T., Phan, T.B., Tran, P.H., et al., 2020a. Effect of Fe (III)-based MOFs on the catalytic efficiency of the tandem cyclooxidative reaction between 2-aminobenzamide and alcohols. New J. Chem. 44 (34), 14529–14535.

Dang, Y.T., Hoang, H.T., Dong, H.C., Bui, K.B.T., Nguyen, L.H.T., Phan, T.B., et al., 2020b. Microwave-assisted synthesis of nano Hf-and Zr-based metal-organic frameworks for enhancement of curcumin adsorption. Microporous Mesoporous Mater. 298, 110064.

Fang, X., Zong, B., Mao, S., 2018. Metal–organic framework-based sensors for environmental contaminant sensing. Nano Micro Lett. 10, 1–19.

Goyal, S., Shaharun, M.S., Kait, C.F., Abdullah, B., 2018. Effect of monometallic copper on zeolitic imidazolate framework-8 synthesized by hydrothermal method. J. Phys. Conf. Ser. 1123 (1), 012062.

Hallquist, M., Wenger, J.C., Baltensperger, U., Rudich, Y., Simpson, D., Claeys, M., et al., 2009. The formation, properties and impact of secondary organic aerosol: current and emerging issues. Atmos. Chem. Phys. 9 (14), 5155–5236.

Harrison, R.M., Yin, J., 2000. Particulate matter in the atmosphere: which particle properties are important for its effects on health? Sci. Total. Environ. 249 (1–3), 85–101.

Hou, M., Gao, J., Yang, L., Guo, S., Li, Y., 2021. Room temperature gas sensing under UV light irradiation for $Ti_3C_2T_x$ MXene derived lamellar TiO_2-C/g-C_3N_4 composites. Appl. Surf. Sci. 535, 147666.

Hsueh, T.J., Hsu, C.L., Chang, S.J., Chen, I.C., 2007. Laterally grown ZnO nanowire ethanol gas sensors. Sens. Actuators B 126 (2), 473–477.

Hsueh, T.J., Chang, S.J., Hsu, C.L., Lin, Y.R., Chen, I.C., 2008. ZnO nanotube ethanol gas sensors. J. Electrochem. Soc. 155 (9), K152.

Karaduman, I., Yıldız, D.E., Sincar, M.M., Acar, S., 2014. UV light activated gas sensor for NO_2 detection. Mater. Sci. Semicond. Process. 28, 43–47.

Li, Z., Zeng, H.C., 2013. Surface and bulk integrations of single-layered Au or Ag nanoparticles onto designated crystal planes {110} or {100} of ZIF-8. Chem. Mater. 25 (9), 1761–1768.

Li, M., Ren, W., Wu, R., Zhang, M., 2017. CeO_2 Enhanced Ethanol Sensing Performance in a CdS Gas Sensor. Sensors 17 (7), 1577.

Li, H., Wang, K., Sun, Y., Lollar, C.T., Li, J., Zhou, H.C., 2018. Recent advances in gas storage and separation using metal–organic frameworks. Mater. Today 21 (2), 108–121.

Li, S., Fu, Q., Pan, C., 2022. A multi-functional wearable sensor based on carbon nanomaterials reinforced TPU fiber with high sensitivity. J. Alloys Compd. 927, 167041.

Liu, X., Oh, M., Lah, M.S., 2011. Adsorbate selectivity of isoreticular microporous metal–organic frameworks with similar static pore dimensions. Cryst. Growth Des. 11 (11), 5064–5071.

Lu, G., Hupp, J.T., 2010. Metal-organic frameworks as sensors: a zif-8 based fabry-perot device as a selective sensor for chemical vapors and gases. J. Am. Chem. Soc. 132 (23), 7832–7833.

Lu, G., Farha, O.K., Zhang, W., Huo, F., Hupp, J.T., 2012. Engineering ZIF-8 thin films for hybrid MOF-based devices. Adv. Mater. 24 (29), 3970–3974.

Mirzaei, A., Leonardi, S.G., Neri, G., 2016. Detection of hazardous volatile organic compounds (VOCs) by metal oxide nanostructures-based gas sensors: a review. Ceram. Int. 42 (14), 15119–15141.

Nguyen, L.H.T., Nguyen, T.T.T., Dang, Y.T., Tran, P.H., Le Hoang Doan, T., 2019. Microwave-assisted synthesis as an efficient method to enhance the catalytic activity of Zr-based metal organic framework UiO-66 in a heterocyclization reaction. Asian J. Org. Chem. 8 (12), 2276–2281.

Ostad, M.I., Shahrak, M.N., Galli, F., 2021. Photocatalytic carbon dioxide reduction to methanol catalyzed by ZnO, Pt, Au, and Cu nanoparticles decorated zeolitic imidazolate framework-8. J. CO2 Util. 43, 101373.

Park, K.S., Ni, Z., Côté, A.P., Choi, J.Y., Huang, R., Uribe-Romo, F.J., et al., 2006. Exceptional chemical and thermal stability of zeolitic imidazolate frameworks. Proc. Natl. Acad. Sci. 103 (27), 10186–10191.

Ren, G., Li, Z., Yang, W., Faheem, M., Xing, J., Zou, X., et al., 2019. ZnO@ ZIF-8 core-shell microspheres for improved ethanol gas sensing. Sens. Actuators B 284, 421–427.

Shoorangiz, M., Shariatifard, L., Roshan, H., Mirzaei, A., 2021. Selective ethanol sensor based on α-Fe_2O_3 nanoparticles. Inorg. Chem. Commun. 133, 108961.

Shukla, S., Ludwig, L., Parrish, C., Seal, S., 2005. Inverse-catalyst-effect observed for nanocrystalline-doped tin oxide sensor at lower operating temperatures. Sens. Actuators B 104 (2), 223–231.

Tan, L.H.D., Kim, J.Y., Lee, J.H., Nguyen, L.H.T., Dang, Y.T., Bui, K.B.T., et al., 2021. Preparation of n-ZnO/p-Co_3O_4 heterojunctions from zeolitic imidazolate frameworks (ZIF-8/ZIF-67) for sensing low ethanol concentrations. Sens. Actuators B 348, 130684.

Tielrooij, K.J., Song, J.C.W., Jensen, S.A., Centeno, A., Pesquera, A., Zurutuza Elorza, A., et al., 2013. Photoexcitation cascade and multiple hot-carrier generation in graphene. Nat. Phys. 9 (4), 248–252.

Tomić, M., Fohlerova, Z., Gràcia, I., Figueras, E., Cané, C., Vallejos, S., 2021. UV-light activated APTES modified WO_3-x nanowires sensitive to ethanol and nitrogen dioxide. Sens. Actuators B 328, 129046.

Tomoda, M., Okano, S., Itagaki, Y., Aono, H., Sadaoka, Y., 2004. Air quality prediction by using semiconducting gas sensor with newly fabricated $SmFeO_3$ film. Sens. Actuators B 97 (2–3), 190–197.

Wu, X., Xiong, S., Mao, Z., Hu, S., Long, X., 2017. A designed ZnO@ ZIF-8 core–shell nanorod film as a gas sensor with excellent selectivity for H_2 over CO. Chem. Eur. J 23 (33), 7969–7975.

Xing, Y., Wang, Z., Zhu, Y., Yan, J., Chen, Y., 2021. High-performance chlorobenzene sensor of bimetallic ZIF-8 (Zn@ Co) based one-dimensional photonic crystals. Phys. Lett. A. 400, 127301.

Xiong, Y., Xu, W., Zhu, Z., Xue, Q., Lu, W., Ding, D., et al., 2017. ZIF-derived porous ZnO-Co_3O_4 hollow polyhedrons heterostructure with highly enhanced ethanol detection performance. Sens. Actuators B 253, 523–532.

Yan, F., Liu, Z.Y., Chen, J.L., Sun, X.Y., Li, X.J., Su, M.X., et al., 2014. Nanoscale zeolitic imidazolate framework-8 as a selective adsorbent for theophylline over caffeine and diprophylline. RSC Adv 4 (62), 33047–33054.

Yang, T.Y., Lin, H.M., Wei, B.Y., Wu, C.Y., Lin, C.K., 2003. UV enhancement of the gas sensing properties of nano-TiO_2. Rev. Adv. Mater. Sci. 4 (1), 48–54.

Young, S.J., Lin, Z.D., Hsiao, C.H., Huang, C.S., 2012. Ethanol gas sensors composed of carbon nanotubes with adsorbed gold nanoparticles. Int. J. Electrochem. Sci. 7 (11), 11634–11640.

Yu, J.B., Sun, M., Yu, M., Yang, M., Yu, H., Yang, Y., et al., 2022. Preparation of near room temperature gas sensor based on regular octahedral porous ZnO/SnO_2 composite. J. Alloys Compd. 920, 165884.

Zhang, Q.X., Ma, S.Y., Zhang, R., Tie, Y., Pei, S.T., 2020. Optimization ethanol detection performance manifested by SnS/SnS_2 nanoparticles. Mater. Lett. 258, 126783.